energies

MDPI

Article

Improved High Temperature Thermoelectric Properties in Misfit $Ca_3Co_4O_9$ by Thermal Annealing

Arindom Chatterjee [1,*], Alexandros El Sachat [2], Ananya Banik [3], Kanishka Biswas [3], Alejandro Castro-Alvarez [4], Clivia M. Sotomayor Torres [1,5], José Santiso [1] and Emigdio Chávez-Ángel [1,*]

[1] Catalan Institute of Nanoscience and Nanotechnology (ICN2), CSIC and BIST, Campus UAB, Bellaterra, 08193 Barcelona, Spain
[2] Institute of Nanoscience and Nanotechnology, National Center for Scientific Research "Demokritos", 15341 Athens, Greece
[3] New Chemistry Unit, School of Advanced Materials, Jawaharlal Nehru Centre for Advanced Scientific Research (JNCASR), Jakkur, Bangalore 06484, India
[4] Laboratorio de Bioproductos Farmacéuticos y Cosméticos, Centro de Excelencia en Medicina Traslacional, Facultad de Medicina, Universidad de La Frontera, Av. Francisco Salazar 01145, Temuco 4780000, Chile
[5] ICREA—Catalan Institute for Research and Advanced Studies, 08010 Barcelona, Spain
* Correspondence: arichatterjee1990@gmail.com (A.C.); emigdio.chavez@icn2.cat (E.C.-Á.)

Abstract: $Ca_3Co_4O_9$, a p-type thermoelectric material based on transition-metal oxides, has garnered significant interest due to its potential in thermoelectric applications. Its unique misfit-layered crystal structure contributes to low thermal conductivity and a high Seebeck coefficient, leading to a thermoelectric figure of merit (zT) of ≥1 at 1000 K. Conventionally, it has been believed that thermopower reaches its upper limit above 200 K. However, our thermopower measurements on polycrystalline $Ca_3Co_4O_9$ samples have revealed an unexpected increase in thermopower above 380 K. In this study, we investigate the effects of high oxygen pressure annealing on $Ca_3Co_4O_9$ and provide an explanation based on the mixed oxide states of cobalt and carrier hopping. Our results demonstrate that annealing induces modifications in the defect chemistry of $Ca_3Co_4O_9$, leading to a decrease in electron hopping probability and the emergence of a thermal activation-like behavior in thermopower. These findings carry significant implications for the design and optimization of thermoelectric materials based on misfit cobaltates, opening new avenues for enhanced thermoelectric performance.

Keywords: $Ca_3Co_4O_9$; thermoelectricity; heike's limit; cobaltates

Citation: Chatterjee, A.; El Sachat, A.; Banik, A.; Biswas, K.; Castro-Alvarez, A.; Sotomayor Torres, C.M.; Santiso, J.; Chávez-Ángel, E. Improved High Temperature Thermoelectric Properties in Misfit $Ca_3Co_4O_9$ by Thermal Annealing. *Energies* **2023**, *16*, 5162. https://doi.org/10.3390/en16135162

Academic Editors: Tingzhen Ming, Yongjia Wu and Yonggao Yan

Received: 31 May 2023
Revised: 30 June 2023
Accepted: 3 July 2023
Published: 4 July 2023

1. Introduction

Misfit cobaltates, such as $Ca_3Co_4O_9$ or Na_xCoO_2, have been the subject of intense research in the field of thermoelectrics due to their high thermoelectric performance at elevated temperatures [1,2]. $Ca_3Co_4O_9$ (CCO) is a promising p-type thermoelectric (TE) material based on transition-metal oxides. This material exhibits a TE figure of merit, $zT \geq 1$ at 1000 K ($zT = S^2/(\rho \cdot \kappa)T$, where ρ represents the electrical resistivity ($\rho = \sigma^{-1}$, where σ is the electrical conductivity), S is the Seebeck coefficient or thermopower, κ is the total thermal conductivity, and T is the absolute temperature) [3]. The high zT in this class of compounds is attributed to two distinct reasons. Firstly, the unique misfit-layered crystal structure of the material results in low in-plane [4] and ultralow out-of-plane thermal conductivity [5]. Secondly, the unique electronic band structure of CCO leads to high S (100–150 μV/K) and low ρ (<10 mΩ.cm) at 300 K [2,6–9].

The misfit-layered crystal structure of CCO is composed of two subunits: a rocksalt-like Ca_2CoO_3 (i.e., CaO-CoO-CaO) and a face-shared CoO_2 octahedra stacked along their c-axis [10,11]. The crystal symmetries of the two subunits differ, causing the cell parameters to not align along all crystallographic axes. A substantial mismatch is observed along the b-axis, where the b-parameter of CoO_2 (b_{CO}) is shorter than the b-parameter of the rocksalt unit (b_{RS}), and their ratio is referred to as the misfit ratio, $q = b_{CO}/b_{RS}$.

This class of compounds, as well as layered Na_xCoO_2, exhibit an intriguing feature wherein thermopower increases linearly with increasing temperature from 10 to 170 K, a behavior typically observed in metallic conductors [12,13]. Beyond 200 K, thermopower becomes temperature independent for misfit cobaltates [14]. Both theoretical and experimental investigations suggest that metallic conduction of travelling charge carriers moving in a broad e_g' band governs thermopower at lower temperatures (T < 150 K), while localized charge carriers in a narrow a_{1g} band dominate at higher temperatures (T > 200 K) [15]. It is generally assumed that thermopower reaches its high-temperature limit above 200 K, as given by Heike's formula [16,17]. However, thermopower measurements (T > 380 K) for polycrystalline samples reveal that thermopower further increases with increasing temperature [14,15,18]. Surprisingly, this increase in thermopower is not due to an increase in resistivity as expected from the single parabolic band model, where both quantities are inversely proportional to charge carrier density. In fact, resistivity decreases within 380–750 K. Thus, it remains unclear why thermopower increases above 380 K, even though it is commonly believed that CCO reaches its high-temperature limit above 200 K [14,19,20]. Numerous hypotheses have been proposed in the literature to explain the observed enhanced S in CCO. These include spin-state transitions in Co^{3+} ions, partial localization of electrons in e_g' orbital, and charge associated with Co-t_{2g} occupancy during structural transitions [13]. However, ab initio calculations have demonstrated that the energy required for the first excited spin in a Co atom is incompatible with the energy scale for a phase transition at 400 K [21]. Instead, they suggest that partial charge localization may be responsible for the observed increase in S. First-principles calculations on CCO indicate that both Ca_2CoO_3 and CoO_2 subunits contribute to the transport, while spectroscopy experiments reveal that the 3d orbital of CoO_6 octahedra in the CoO_2 layer participates in conduction [8]. Further analysis of the crystal structures at higher temperatures suggested that the structural transition occurs due to the arrangement of CoO layer in the RS sub-unit, which weakly modifies the CoO_2 layer, thereby explaining the resistivity drop but not the increased S [22]. Despite numerous proposed explanations, the fundamental mechanism that drives the observed increase in the parameter "S" beyond 380 K remains unclear.

This study examines the impact of high oxygen pressure annealing on the electronic transport and thermoelectric properties of polycrystalline pellets of CCO. Specifically, we have demonstrated that the temperature-independent behaviour of thermopower in as-synthesized samples can be altered to exhibit a normal thermal activation-like behaviour through annealing.

To explore these effects, we conducted electronic transport and thermoelectric property measurements on as-synthesized and annealed samples over a wide temperature range (310–750 K). Our analysis revealed that the thermopower of the as-synthesized samples remained constant over a temperature range of 320–380 K, and then increased with increasing temperature from 380 to 750 K. In contrast, the annealed samples did not exhibit any saturation in thermopower, but rather displayed a thermal activation-like behaviour across the entire range of temperatures studied.

To explain these observations, we propose a plausible mechanism based on the hopping probability of electrons based on the Heike's limit of the Seebeck coefficient. Our results suggest that high oxygen pressure annealing may alter the defect chemistry of CCO, resulting in a reduction in the hopping probability of electrons and the emergence of a thermal activation-like behaviour in thermopower. These findings have important implications for the design and optimization of CCO-based thermoelectric materials.

2. Experimental Methods

Synthesis: $Ca_3Co_4O_9$ polycrystalline pellets were synthesized by conventional high temperature solid state reactions [23,24]. Stoichiometric mixtures of Co_3O_4 and $CaCO_3$ were homogenized using an agate mortar to obtain a homogeneous powder. The powder was pressed into a pellet using a stainless-steel die under uniaxial pressures, followed by calcination and sintering in a high O_2 atmosphere. The calcined pellet was finely ground,

pressed into a new pellet, and sintered in a tubular furnace at 900 °C for 20 h in a 100 sccm oxygen flow. The density of cold-pressed samples was found to be approximately 87% relative to the theoretical value. To enhance the density to above 90%, which is necessary for achieving reliable electronic, thermoelectric, and thermal transport properties [25–28], spark-plasma sintering was conducted. Specifically, the sintering process was carried out at a uniaxial press of ~40 MPa at 923 K temperature. The final density achieved after spark-plasma sintering was approximately 91.8% relative to the theoretical value.

Thermoelectric measurements: The resulting spark plasma-sintered pellets were prepared for the thermoelectric characterization through two means: (i) rectangular bars of dimensions 10 × 2.5 × 2 mm^3 were fabricated for the measurement of S and ρ through the standard 4-probe method using a LINSEIS instrument (Selb, Germany), under a controlled helium atmosphere (0.1 MPa) between 310 and 750 K, and (ii) disks of diameter 8 mm and thickness of 3 mm were cut for the measurement of thermal diffusivity using laser flash techniques in a NETZSCH LFA instrument (Selb, Germany) under a controlled nitrogen atmosphere between 300 and 750 K. To optimize the heat fluxes, both sides of the disks were coated with carbon. The total thermal conductivity was calculated using the relation $\kappa_{total} = D \cdot C_p \cdot d$, where D, C_p, and d are the thermal diffusivity, specific heat capacity, and density of the pellet, respectively.

Estimation of the ratio of particles to sites using Heikes equation: The continous increase of the S in CCO materials was estimated using the Heike's formula given as follows [16]:

$$S_{T\to\infty} = -\frac{k_B}{e} ln\left(\frac{\frac{N}{N_A}}{1-\frac{N}{N_A}}\right) = -\frac{k_B}{e} ln\left(\frac{x}{1-x}\right) \quad (1)$$

where x denotes the ratio of number of particles (N) to sites (N_A) and e is the absolute value of elementary electron charge. x was estimated by using the measured Seebeck of each temperature, i.e.,

$$x = \frac{\exp(-\alpha)}{1+\exp(-\alpha)},\ \alpha = \frac{e \cdot S}{k_B} \quad (2)$$

Estimation of the activation energy: The activation energy (E_A) of the system was determined using the small polaron hopping model (or Arrhenius type model) as follows [29]:

$$\sigma(T) = \frac{\sigma_0}{T} \exp\left(-\frac{E_A}{k_B T}\right) \quad (3)$$

where $\sigma(T)$ represents the electrical conductivity at temperature T, σ_0 is a pre-exponential factor (or residual resistivity), and k_B is the Boltzmann constant. By taking the natural logarithm of the electrical conductivity multiplied by the measured temperature ($\ln(\sigma \cdot T)$) and plotting it against the reciprocal of temperature ($1/T$), the slope of this linear relationship provides a direct measure of the activation energy as follows:

$$\ln(\sigma \cdot T) = -\frac{E_A}{k_B}\frac{1}{T} + \ln(\sigma_0) \quad (4)$$

Structural characterization: The samples underwent structural characterization using X-ray diffraction (XRD) (from PANalytical X'pert Pro MPD diffractometer, Malvern, UK). The XRD analysis allowed for the determination of the crystal structure and lattice parameters of the material. Additionally, elemental analysis was performed using an EDX detector (Quanta 650 FEG, Hillsboro, OR, USA) to determine the chemical composition of the material. The quantification and oxidation states of cobalt ions were also determined using X-ray photoelectron spectroscopy (XPS). XPS measurements were conducted using a SPECS PHOIBOS150 hemispherical analyzer (Berlin, Germany) equipped with a monochromatic X-ray source operating at 1486.6 eV and a power of 300 W. The synthesized samples were polycrystalline, and hence, no preferred orientations were observed in their crystal

structure. Therefore, anisotropies were not found in the thermal and electronic properties of the samples.

Annealing: To investigate the effect of annealing on the thermoelectric properties of the $Ca_3Co_4O_9$ polycrystalline pellets, the as-synthesized sample was measured in a controlled helium atmosphere up to 710 K and then cooled down to room temperature with the same controlled atmosphere. The heating–cooling cycle from 300 to 710 K usually takes a few hours. Then, the sample was annealed at 1173 K for 120 min at 20 sccm oxygen flow. We call this sample "air-annealed". The thermoelectric measurements of air-annealed sample were performed in the same controlled helium atmosphere within 300–710 K, and cooled down as before. The "air-annealed" sample was annealed again at 1173 K for 120 min at 100 sccm oxygen flow. We call this sample "oxygen-annealed". Then, transport properties of oxygen-annealed sample were measured in the same helium atmosphere as before. By performing transport measurements under different annealing conditions, we aimed to gain insights into the changes in the electronic and thermoelectric properties of $Ca_3Co_4O_9$ as a function of annealing conditions. After annealing, no significant variations in the XRD patterns were observed, suggesting that the material retained its crystal structure and stability under the given annealing conditions. Figure 1 presents a flow chart illustrating the distinct stages involved in the measurements process of the $Ca_3Co_4O_9$ compounds.

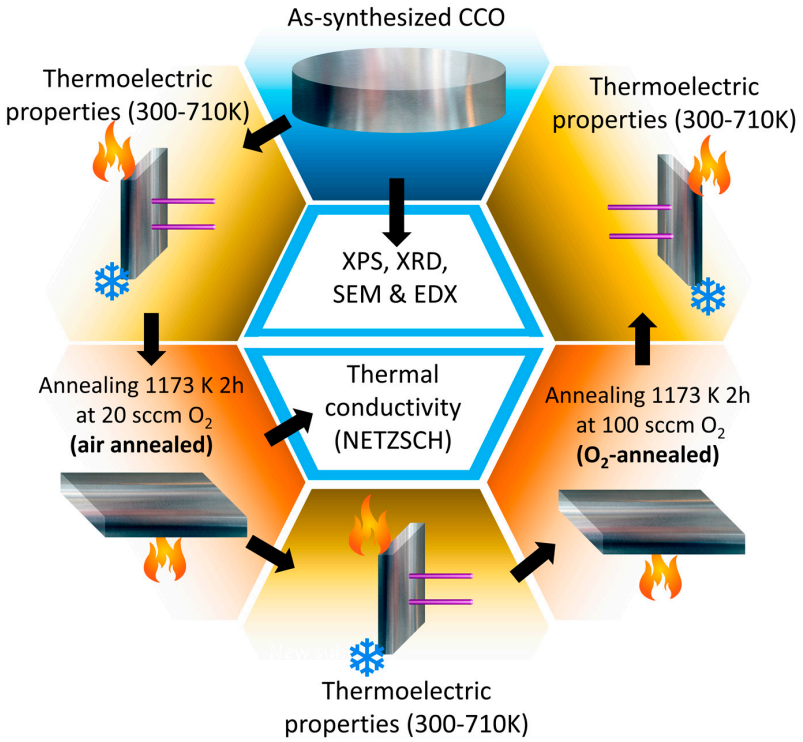

Figure 1. Flow chart outlining the sequential steps undertaken throughout the experimental investigation.

3. Results

3.1. Structural and Elemental Characterizations

The inset of Figure 2a shows a schematic representation of CCO system, which serves to elucidate its structural arrangement and layered nature. The crystal structure of CCO exhibits a misfit-layered configuration, characterized by the presence of alternating rocksalt layers (Ca_2CoO_3) and face-shared octahedra layers (CoO_2). This figure further highlights the three-dimensional stacking of these layers and their unique arrangement. Complementing this illustration, Figure 2a,b present the powder X-ray diffraction (XRD) patterns obtained from the as-synthesized CCO sample. Notably, the XRD pattern closely resembles those observed in previous studies on polycrystalline CCO samples synthesized by other researchers [30,31]. The peak assignment was carried out based on the

work of Hira et al. [32]. The analysis of the XRD data reveals the absence of detectable impurity phases.

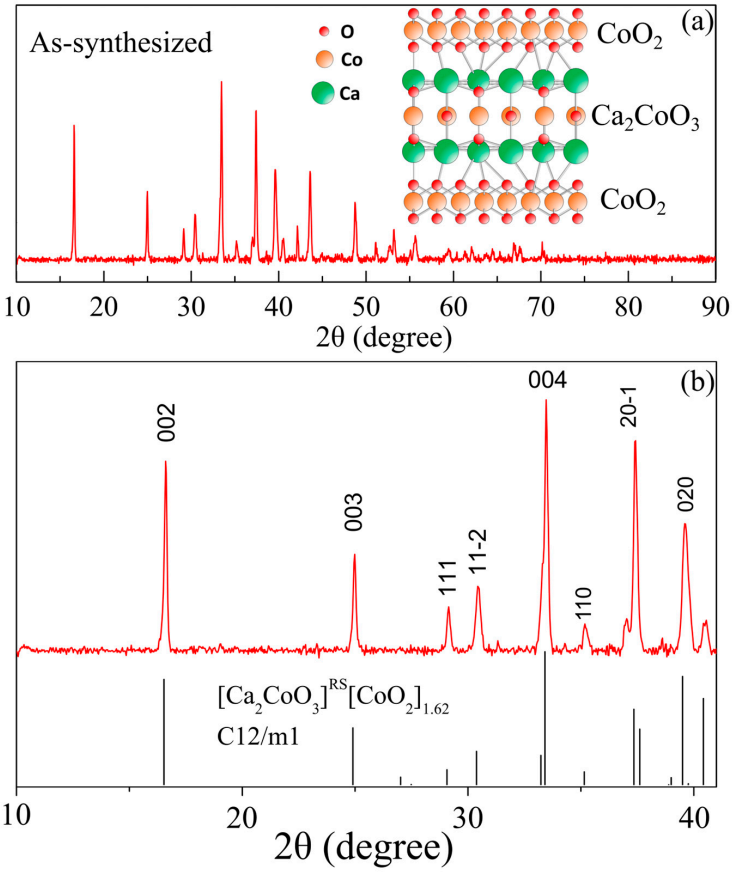

Figure 2. Inset: schematic representation of the misfit-layered crystal structure of $Ca_3Co_4O_9$ illustrating the arrangement of the two subunits: Ca2CoO3, which consists of CaO-CoO-CaO layers, and a face-shared network of CoO_2 octahedra. (**a**) XRD of as-synthesized sample full range and (**b**) zoom around 10 to 40 degrees. The peak assignment was carried out based on the work of Hira et al. [32].

Figure 3a,b show the EDX analysis of the as-synthesized sample and SEM picture of the CCO powder showing a particle size around few micrometers. EDX analysis reveals the elemental composition of the as-synthesized sample. The spectrum obtained shows the characteristic peaks corresponding to calcium, cobalt, and oxygen atoms presented in the CCO compound. The carbon peak shown at low energy corresponds to the carbon tape used to hold the sample.

Figure 4 gives essential insights into the elemental composition and oxidation states of the material under investigation. In Figure 4a, the XPS spectrum clearly demonstrates the presence of all three elements, namely Ca, O, and Co [33]. In order to gain a deeper understanding of the oxidation states of cobalt ions, a high-resolution XPS measurement was conducted targeting the Co-2p region (770–810 eV), as shown in Figure 4b–d. The raw spectrum (black line) is presented at the top, while the baseline-corrected spectrum is displayed at the bottom of Figure 4b. Notably, two prominent peaks corresponding to Co $2p_{3/2}$ and $2p_{1/2}$ are clearly discernible, accompanied by two additional satellite peaks located at relatively higher binding energies. These satellite peaks are commonly attributed to the presence of mixed valence states of cobalt ions [29]. By performing meticulous fitting of the Co-2p spectrum (Figure 4c,d), three distinct peaks with noticeable variations in their binding energies, full width at half maximum (FWHM), and area under the curve were identified. Based on these distinctive characteristics, we confidently assigned these peaks to the presence of Co^{2+}, Co^{3+}, and Co^{4+} ions [34]. It is noteworthy that the observed

shift of binding energies towards higher energies with increasing oxidation states aligns with expectations. The coexistence of mixed valence states, including Co^{2+} ions in the rock salt layer and a combination of Co^{3+} and Co^{4+} ions in the hexagonal layer, not only provides insights into the material's composition but also enhances our understanding of its oxidation states [34].

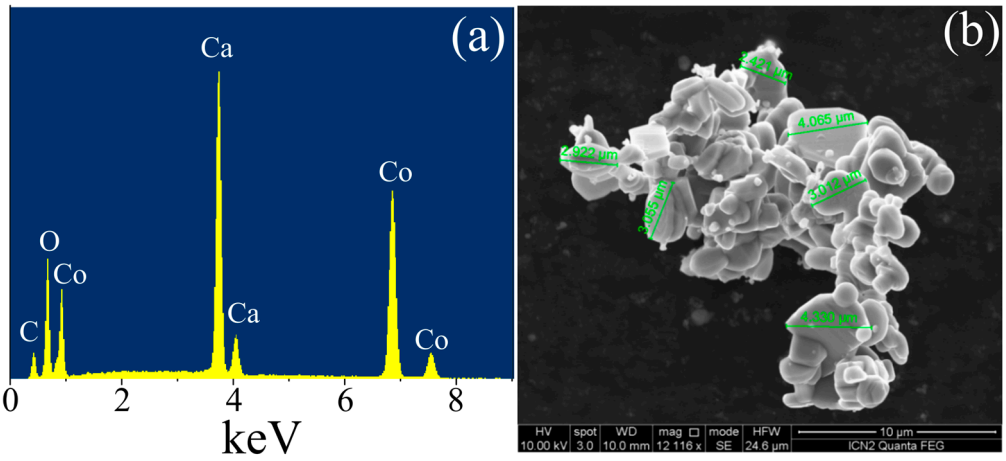

Figure 3. (**a**) Elemental analysis by energy dispersive X-ray spectroscopy (EDX). (**b**) SEM picture of the CCO powder.

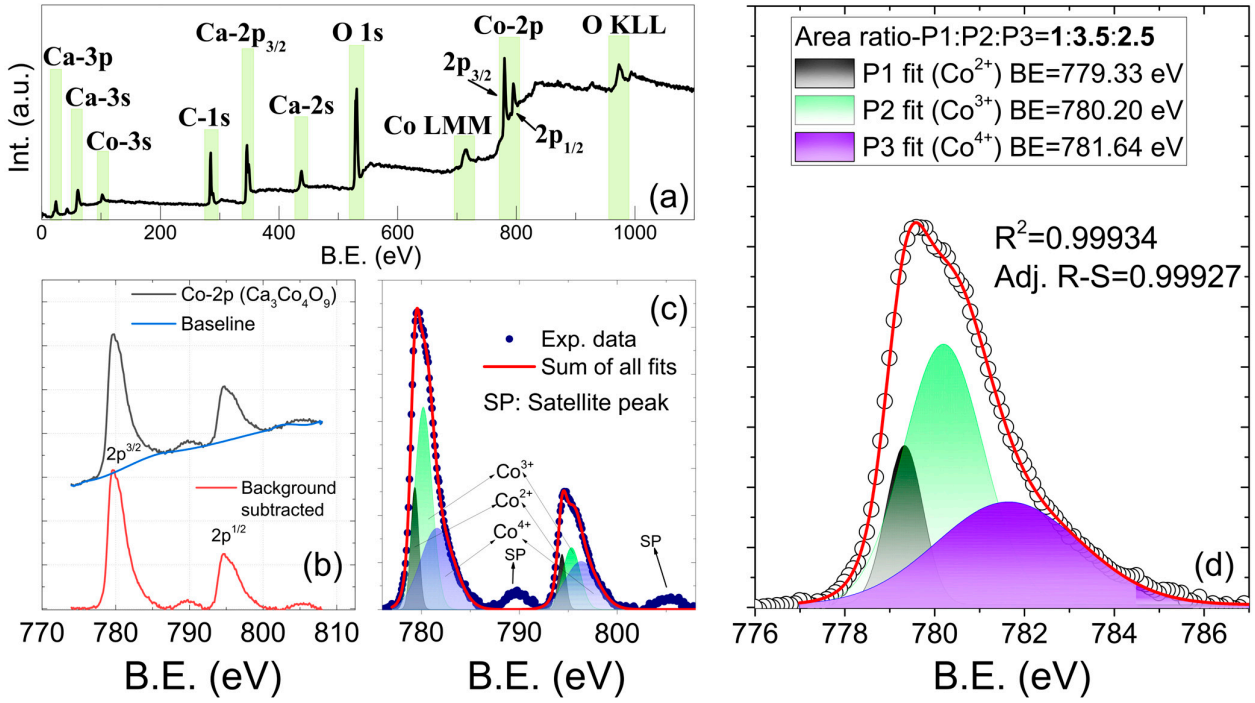

Figure 4. XPS spectrum of as-sythesid sample. (**a**) Full range and zoom around Co-2p oxidation state: (**b**) raw and baselined data, (**c**) baselined and fitted spectrum, (**d**) zoom to highlight the goodness of the fitted spectrum.

3.2. Electronic Transport Properties and Thermoelectric Power

Figure 5a,c show the simultaneous measurements of resistivity (ρ(T)) and thermopower (S(T)) as a function of temperature. ρ(T) displays a non-monotonic behavior for the as-synthesized sample. Initially, within the temperature range of 300–500 K, it decreases from 21 to 18 mΩ·cm. However, beyond this range, it continuously increases to 22.6 mΩ·cm at 710 K. In contrast, S(T) exhibits a positive value of 140 mV/K at 330 K, indicating the

prevalence of p-type charge carriers in the samples. Moreover, it remains temperature independent between 310 K and 380 K but increases beyond this range to reach a maximum value of 194 mV/K at 710 K, which is consistent with previous reports [18,35,36]. The air-annealed sample exhibited a similar behavior of resistivity (ρ) within the temperature range of 330–380 K when compared to the as-synthesized sample. However, resistivity decreased from 22 to 17 mΩ.cm with increasing temperature up to 710 K, displaying a thermal activation-like behavior (see Figure 5b). In contrast, the absolute value of thermopower and its temperature dependence remained comparable to the as-synthesized sample, implying that high-temperature conductivity was mainly improved by annealing process. In standard band gap materials, electronic resistivity and thermopower decrease with increasing temperature. However, in the as-synthesized sample, we observed that the thermopower increases with temperature while the resistivity decreases. This observation suggests that electronic resistivity and thermopower may be governed by different mechanisms.

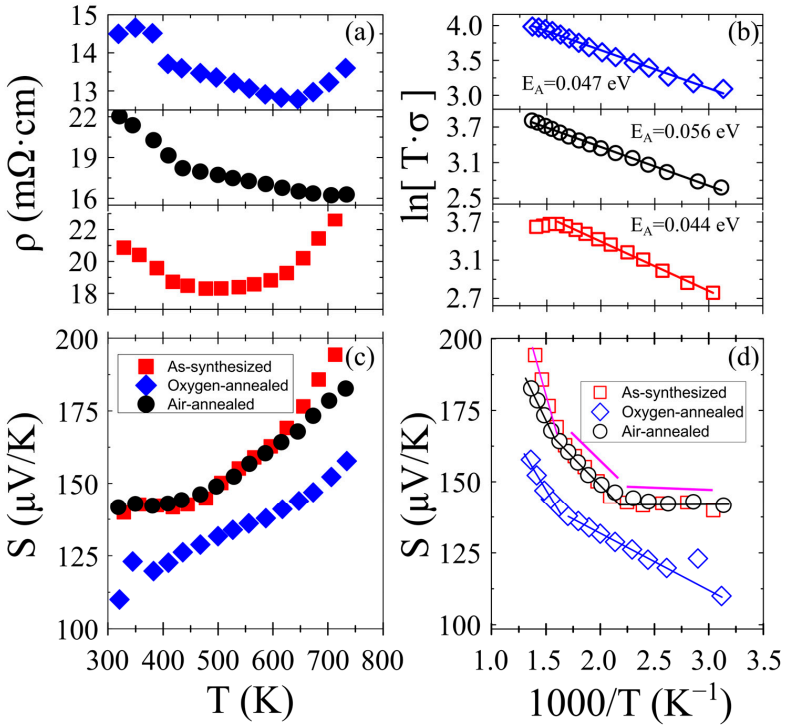

Figure 5. (**a**) Electrical resistivity of as-synthesized (red square), oxygen-annealed (blue diamond), and air-annealed CCO samples as function of tempertature. (**b**) Linear fitting of ln(σ·T) versus 1000/T for each sample. (**c**,**d**) Seebeck coefficient of the set of samples as function of temperature.

To investigate this further, we performed high temperature transport measurements of the oxygen-annealed sample. The results shows a significant drop in ρ to 14 mΩ.cm, while their temperature dependence remain constant between 300 K and 380 K. The observed reduction in resistivity in our sample could be attributed to an increase in the density of charge carriers, an improvement in charge mobility, or a combination of both. It is plausible that the annealing process at high oxygen pressure resulted in the compensation of oxygen vacancies, leading to the introduction of extra charge carriers (i.e., holes or Co^{+4} ions) in the CCO lattice. Oxygenation may occur within the rock salt type $Ca_2CoO_{3-\delta}$ layer [37], and the charge neutrality is then balanced by producing a higher ratio of Co^{+4}/Co^{+3} ions in CoO_2 via charge transfer from the rock salt layer to the CoO_2 sub-unit [38]. In contrast, the *S* of the sample decreased to +110 μ V/K at 330 K, but its temperature dependence remained relatively stable. This observation is consistent with the general understanding that in the majority of thermoelectric materials, the electronic conductivity is directly proportional to the concentration of charge carriers, while the thermopower is inversely proportional to it. Thus, this observation further supports the hypothesis that the

annealing process introduced additional holes in the CCO material, thereby enhancing its electrical conductivity.

Moreover, the activation energy (E_A) was determined thorough the analysis of the slope obtained from plotting the natural logarithm of the temperature dependence of resistivity multiplied by the temperature ($\ln(T \cdot \sigma)$) against the reciprocal of temperature ($1/T$) (see Figure 5b and Equation (4)). In a system characterized by coherent charge carriers, the obtained E_A values from both curves are expected to exhibit close resemblance. However, any significant deviation between these values suggests the possibility of incoherent transport as a function of temperature. This implies that the carriers in the system are localized in nature and primarily follow a hopping transport mechanism.

Furthermore, the activation energy (E_A) obtained from the temperature dependence of resistivity $\ln(\sigma \cdot T)$ and thermopower S(T) as a function of $1/T$ was analysed using Equation (4), as shown in Figure 5b,d. In a system with coherent charge carriers, the E_A obtained from both curves should be very similar to each other. If not, that might indicate a sign of incoherent transport as a function of temperature, implying that carriers are localized in nature and mainly obey hopping transport mechanism [14,39]. The localized nature of charge carriers at high enough temperature produces temperature-independent thermopower, as explained by the Heike's formula (or sometimes referred to as the Mott-Heikes formula, see Equation (1)) [40].

Figure 6 shows the schematic representation of the electronic structure of misfit cobaltates. The 3d orbitals of the Co atom in the CoO_2 layer experience splitting into t_{2g} and e_g energy states due to the octahedral crystal field. Moreover, the t_{2g} orbitals undergo further splitting into a narrow out-of-plane a_{1g} band and a wide in-plane $e_{g'}$ band due to the triangular distortion present in the CoO_2 layer [21]. The conduction mechanism at lower temperatures ($T < 200$ K) is dominated by the $e_{g'}$ band, which has a broad width [8]. Conversely, at relatively higher temperatures ($T > 200$ K), the narrow a_{1g} band dominates the conduction mechanism [21]. Due to its narrow bandwidth, the charge carriers become localized, and the conduction mechanism is governed by the hopping of charge carriers from one site to another. It is noteworthy that ρ decreases slightly or remains temperature-independent for all samples within the range of 310–750 K. Limelette et al. [41] proposed the opening of a pseudogap, which is caused by the disappearance of the quasiparticle resonance. Hence, a slight increase in the charge carrier concentration (n) within the range of 310–750 K or a fixed number can be considered. At temperatures below 10 K, previous studies proposed the inclusion of a spin-entropy contribution to the thermopower in misfit [42] and Na_xCoO_2 cobaltates [43,44]. The S shows a linear increase in the range of 20–180 K, indicating metallic conduction, followed by a temperature-independent behavior in the range of 180–380 K, suggesting that S reached its high temperature limit [21,45], as previously discussed. At extremely high temperatures ($T \rightarrow \infty$), the band width, W, becomes narrow, and consequently, charge carriers are localized. Thus, in this limit (when $k_BT \gg W$, where k_B is the Boltzmann constant), S becomes a function of a pure thermodynamic parameter, the configurational entropy, which is related to the degeneracy of the charge carriers over the available sites. Within this regime, Heike's formula was derived as a mathematical expression for S, considering that 'N' number of particles are distributed over 'N_A' sites, where two particles cannot occupy the same site (Equation (1)). Although this formula was modified by including the spin-orbit degeneracy [45] as an extra contribution to S, it remains unclear [46]. Intriguingly, our measurements suggest that S continues to increase with temperature from 380 to 750 K, and therefore, the actual high temperature limit for CCO remains unresolved.

A structural phase transition at around 400 K has been reported in CCO, as evidenced by lattice parameters (a, b_1, and b_2), resistivity, and specific heat exhibiting a hysteresis behavior with a magnetic field, indicating the possible presence of magnetic ordering [22,36,43]. Furthermore, magnetic phase transitions have been observed at higher temperatures. For instance, a transition from low-spin Co^{3+} (LS-Co^{3+}) to intermediate-spin

Co^{3+} (IS-Co^{3+}) is postulated to occur at 400 K [47,48], while another phase transition from paramagnetic LS-Co^{3+} to paramagnetic high-spin (HS) state was reported at 500 K [41].

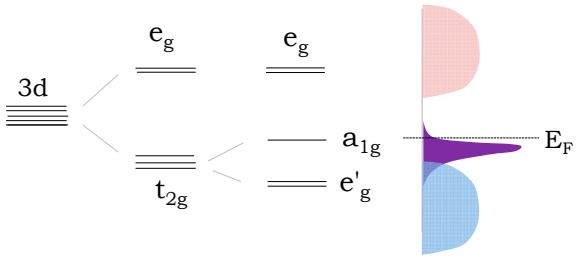

Figure 6. Schematic representation of electronic structure of $Ca_3Co_4O_9$.

The investigation of the temperature-dependent behavior of the S beyond 380 K, via Heike's formula, is a subject of interest, given its potential to offer valuable insights into the transition of partial LS-Co^{+3} to an IS-Co^{+3} configuration at elevated temperatures. Equation (1) indicates that S is temperature independent and solely reliant on the parameter x. If Heike's formula is valid between 200 and 710 K, then the rise of S can be explained by the decrease of x. The variation of 'x' between 310 and 710 K was calculated from the measured S, using Equation (2), as shown in Figure 7a. The results indicate that for as-synthesized and air-annealed, 'x' should decrease from 0.16 to 0.09 within the temperature range of 310–710 K to explain the increase of S from 140 to 195 μV/K. The decrease of 'x' with increasing temperature is possible if either 'N' decreases or N_A increases. Based on ρ (T), we assumed that either [n] increases slightly or remains almost constant. In either scenario, N_A must increase to augment S. For the purpose of simplicity, we have considered N as a constant $N = [n] \times V_{unit\ cell}$, where $V_{unit\ cell}$ is the volume of the unit cell.

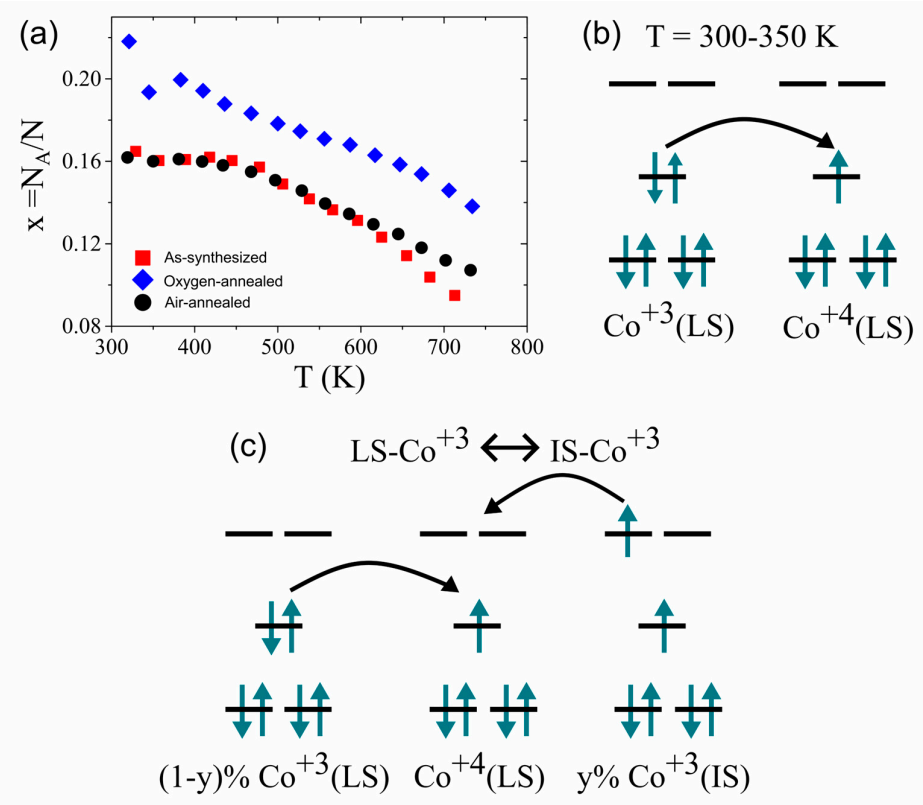

Figure 7. High temperature limit of thermopower and Heike's formula. (**a**) Calculated x (i.e., ratio of particle to site) from measured S from 300 to 750 K. Solid lines are guide to the eyes. (**b**) Hopping of LS-Co^{+4} electrons in LS-Co^{+3} background at 300–350 K and (**c**) hopping of LS-Co^{+4} in the LS-Co^{+3} and IS-Co^{+3} background at 550 K (or T > 380 K).

In the temperature range of 300–350 K, the conduction mechanism in the system can be explicated by the a_{1g} electron hopping between the LS-Co^{+3} and LS-Co^{+4} states, as depicted in Figure 7b. We assume that a y% of LS-Co^{+3} undergoes a spin-state transition from LS to IS-Co^{+3}, and the remaining (1−y)% stays as LS-Co^{+3} by reaching an equilibrium at higher temperatures (see Figure 7c). Therefore, the presence of both LS and IS-Co^{+3} ions changes the probability of Co^{+4} electron (or hole) hopping. For temperatures above 380 K, a_{1g} electrons of LS-Co^{+3} can hop within the a_{1g} state of LS-Co^{+4}, while the e_g electrons of IS-Co^{+3} ions can also hop into the e_g states of LS-Co^{+4}, as indicated by arrows.

After the spin-state transition, two situations can be highlighted: (i) holes in LS-Co^{+4} can hop in the background of both LS-Co^{+3} and IS-Co^{+3}, resulting in an increase in hopping probability, and (ii) the N_A sites is also increased as e_g energy states participate in hopping. Consequently, it can be argued that the enhanced hopping probability of electrons at higher temperatures reduces the resistivity, and the increased number of N_A reduces the value of x, which could eventually increase the Seebeck coefficient with temperature. However, this is merely a hypothesis, and further experiments are necessary to obtain better insights into the transport mechanism at higher temperatures. For comparison, power factors (S^2/ρ or σS^2) of the as-synthesized and annealed samples are plotted together in Figure 8a. All the samples displayed a nearly identical power factor from 210 to 600 K. The 20-sccm oxygen-annealed sample at 710 K exhibited a considerable enhancement. The thermal conductivity of the air-annealed sample is displayed in Figure 8b. Both heating up and colling down measurements showed quite similar results and constant temperature depedence. The quite low κ of the misfit cobaltates is mainly attributed to the phonon scattering at the CoO_2 and RS interfaces and the highly ordered RS layer [49]. However, the lower κ for polycrystalline samples reflects the important contribution of phonon scattering at the grain boundaries [9].

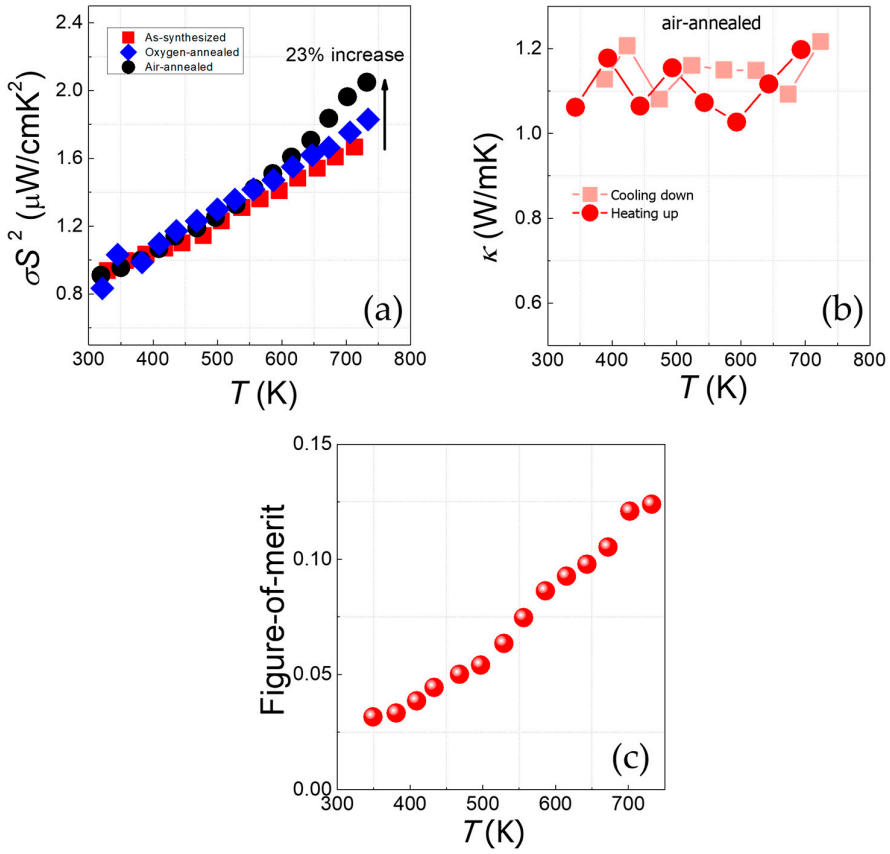

Figure 8. (**a**) Power factor of as-synthesized (red square), oxygen-annealed (blue diamond), and air-annealed CCO samples as function of tempertature. (**b**) Measured thermal conductivity of air-anealed sample and funtion of temperature. (**c**) Thermoelectric figure of merit of the air-annealed sample.

4. Conclusions

This study focused on the preparation and thermoelectrical characterization of polycrystalline bulk $Ca_3Co_4O_9$ samples subject to different annealing processes subject to different oxygen pressures. The thermoelectric properties of both as-synthesized and annealed samples are observed to be highly stable within the temperature range of 310–750 K. The influence of oxygen pressure on the electronic resistance and thermoelectric power was investigated through post-annealing at high temperatures. The results demonstrated that the oxygen-annealed sample exhibited metallic resistivity, lower resistance, and the absence of temperature-independent thermopower. The spin-state transition of cobalt ions was identified as a crucial factor affecting the hopping probability of localized carriers and its potential correlation with temperature-dependent thermopower. Furthermore, the air-annealed (atmosphere with low O_2 pressure) sample showcased a notable 23% enhancement in power factor at 750 K compared to the as-synthesized sample. These findings shed light on the intricate relationship between oxygen pressure, cobalt ion spin states, and the thermoelectric properties of $Ca_3Co_4O_9$, contributing to the understanding and advancement of thermoelectric materials for various applications.

Author Contributions: Conceptualization, C.M.S.T., J.S. and E.C.-Á.; data curation, A.C., A.B. and K.B.; formal analysis, A.C., A.B., K.B. and E.C.-Á.; funding acquisition, C.M.S.T. and J.S.; investigation, A.C., A.E.S., A.B., A.C.-A. and E.C.-Á.; methodology, A.C.; resources, C.M.S.T. and J.S.; software, A.C.-A.; supervision, C.M.S.T. and J.S.; validation, A.E.S.; writing—original draft, A.C. and E.C.-Á.; writing—review and editing, A.C., A.E.S., A.C.-A. and E.C.-Á. All authors have read and agreed to the published version of the manuscript.

Funding: This research was funded by MINECO ref. MAT2016-77100-C2-1-P; CNRS-CSIC PICS Project ref. 261091, the EU for funding through project H2020-MSCA-RISE-2014 ref. 645658, and the AGAUR agency for 2017SGR. ICN2 is funded by the CERCA program/Generalitat de Catalunya and by the Severo Ochoa program of the Spanish Ministry of Economy, Industry and Competitiveness (MINECO, grant no. SEV-2017-0706). C.M.S.T. and E.C.-Á. acknowledge support from Spanish Ministry MINECO/FEDER: FIS2015-70862-P PHENTOM. A.E.S. acknowledges funding from the EU-H2020 research and innovation program under the Marie Sklodowska Curie Individual Fellowship THERMIC (Grant No. 101029727).

Data Availability Statement: Raw data can be provided by the corresponding and first author (A.C.) upon reasonable request.

Conflicts of Interest: The authors declare no conflict of interest.

References

1. Brinks, P.; Huijben, M. Thermoelectric Oxides. In *Epitaxial Growth of Complex Metal Oxides*; Elsevier: Amsterdam, The Netherlands, 2015; pp. 397–441.
2. Yu, J.; Freer, R. Calcium Cobaltite, a Promising Oxide for Energy Harvesting: Effective Strategies toward Enhanced Thermoelectric Performance. *J. Phys. Energy* **2022**, *4*, 022001. [CrossRef]
3. Terasaki, I. Research Update: Oxide Thermoelectrics: Beyond the Conventional Design Rules. *APL Mater.* **2016**, *4*, 104501. [CrossRef]
4. Satake, A.; Tanaka, H.; Ohkawa, T.; Fujii, T.; Terasaki, I. Thermal Conductivity of the Thermoelectric Layered Cobalt Oxides Measured by the Harman Method. *J. Appl. Phys.* **2004**, *96*, 931–933. [CrossRef]
5. Li, L.; Yan, X.-J.; Dong, S.-T.; Lv, Y.-Y.; Li, X.; Yao, S.-H.; Chen, Y.-B.; Zhang, S.-T.; Zhou, J.; Lu, H.; et al. Ultra-Low Thermal Conductivities along c-Axis of Naturally Misfit Layered $Bi_2[AE]_2Co_2O_y$ (AE = Ca, $Ca_{0.5}Sr_{0.5}$, Sr, Ba) Single Crystals. *Appl. Phys. Lett.* **2017**, *111*, 033902. [CrossRef]
6. Singh, D.J. Electronic Structure of $NaCo_2O_4$. *Phys. Rev. B* **2000**, *61*, 13397–13402. [CrossRef]
7. Kuroki, K.; Arita, R. "Pudding Mold" Band Drives Large Thermopower in Na_XCoO_2. *J. Phys. Soc. Jpn.* **2007**, *76*, 3–6. [CrossRef]
8. Takeuchi, T.; Kondo, T.; Takami, T.; Takahashi, H.; Ikuta, H.; Mizutani, U.; Soda, K.; Funahashi, R.; Shikano, M.; Mikami, M.; et al. Contribution of Electronic Structure to the Large Thermoelectric Power in Layered Cobalt Oxides. *Phys. Rev. B* **2004**, *69*, 125410. [CrossRef]
9. Chatterjee, A.; Banik, A.; El Sachat, A.; Caicedo Roque, J.M.; Padilla-Pantoja, J.; Sotomayor Torres, C.M.; Biswas, K.; Santiso, J.; Chavez-Angel, E. Enhanced Thermoelectric Properties of Misfit $Bi_2Sr_{2-X}Ca_xCo_2O_y$: Isovalent Substitutions and Selective Phonon Scattering. *Materials* **2023**, *16*, 1413. [CrossRef] [PubMed]

10. Lambert, S.; Leligny, H.; Grebille, D. Three Forms of the Misfit Layered Cobaltite $[Ca_2CoO_3]$ $[CoO_2]_{1.62}$·A 4D Structural Investigation. *J. Solid State Chem.* **2001**, *160*, 322–331. [CrossRef]
11. Iyazaki, Y.M.; Noda, M.O.; Ku, T.O.; Ikuchi, M.K.; Shii, Y.I. Modulated Structure of the Thermoelectric Compound $[Ca_2CoO_3]_{0.62}CoO_2$. *J. Phys. Soc. Jpn.* **2002**, *71*, 491–497. [CrossRef]
12. Terasaki, I.; Sasago, Y.; Uchinokura, K. Large Thermoelectric Power in $NaCo_2O_4$ Single Crystals. *Phys. Rev. B* **1997**, *56*, R12685–R12687. [CrossRef]
13. Masset, A.; Michel, C.; Maignan, A.; Hervieu, M.; Toulemonde, O.; Studer, F.; Raveau, B.; Hejtmanek, J. Misfit-Layered Cobaltite with an Anisotropic Giant Magnetoresistance. *Phys. Rev. B—Condens. Matter Mater. Phys.* **2000**, *62*, 166–175. [CrossRef]
14. Sakabayashi, H.; Okazaki, R. Crossover from Itinerant to Localized States in the Thermoelectric Oxide $[Ca_2CoO_3]_{0.62}[CoO_2]$. *Phys. Rev. B* **2021**, *103*, 125119. [CrossRef]
15. Kuno, S.; Takeuchi, T.; Ikuta, H.; Kondo, T.; Kaminski, A.; Saito, Y.; Fujimori, S. Electronic Structure and Thermoelectric Properties of a Layered Cobalt Oxide Na_xCoO_2 ($0.5 << x << 0.8$) Investigated by Angle-Resolved Photoemission Spectroscopy. In Proceedings of the 2007 26th International Conference on Thermoelectrics, Jeju, Republic of Korea, 3–7 June 2007; IEEE: Piscataway, NJ, USA, 2007; Volume 2, pp. 99–102.
16. Chaikin, P.M.; Beni, G. Thermopower in the Correlated Hopping Regime. *Phys. Rev. B* **1976**, *13*, 647–651. [CrossRef]
17. Koshibae, W.; Tsutsui, K.; Maekawa, S. Thermopower in Cobalt Oxides. *Phys. Rev. B* **2000**, *62*, 6869–6872. [CrossRef]
18. Van Nong, N.; Pryds, N.; Linderoth, S.; Ohtaki, M. Enhancement of the Thermoelectric Performance of P-Type Layered Oxide $Ca_3Co_4O_{9+\delta}$ through Heavy Doping and Metallic Nanoinclusions. *Adv. Mater.* **2011**, *23*, 2484–2490. [CrossRef]
19. Amin, B.; Eckern, U.; Schwingenschlögl, U. Thermoelectric Properties of the Misfit Cobaltate $Ca_3Co_4O_9$. *Appl. Phys. Lett.* **2017**, *110*, 233505. [CrossRef]
20. Paul, B.; Schroeder, J.L.; Kerdsongpanya, S.; Van Nong, N.; Schell, N.; Ostach, D.; Lu, J.; Birch, J.; Eklund, P. Mechanism of Formation of the Thermoelectric Layered Cobaltate $Ca_3Co_4O_9$ by Annealing of CaO-CoO Thin Films. *Adv. Electron. Mater.* **2015**, *1*, 1400022. [CrossRef]
21. Soret, J.; Lepetit, M.B. Electronic Structure of the $Ca_3Co_4O_9$ Compound from Ab Initio Local Interactions. *Phys. Rev. B—Condens. Matter Mater. Phys.* **2012**, *85*, 165145. [CrossRef]
22. Muguerra, H.; Grebille, D. Original Disorder-Order Transition Related to Electronic and Magnetic Properties in the Thermoelectric Misfit Phase $[Ca_2CoO_3][CoO_3]_{1.62}$. *Acta Crystallogr. Sect. B Struct. Sci.* **2008**, *64*, 676–683. [CrossRef]
23. Wang, D.; Chen, L.; Yao, Q.; Li, J. High-Temperature Thermoelectric Properties of $Ca_3Co_4O_{9+\delta}$ with Eu Substitution. *Solid State Commun.* **2004**, *129*, 615–618. [CrossRef]
24. Wu, N.; Holgate, T.C.; Van Nong, N.; Pryds, N.; Linderoth, S. High Temperature Thermoelectric Properties of $Ca_3Co_4O_{9+\delta}$ by Auto-Combustion Synthesis and Spark Plasma Sintering. *J. Eur. Ceram. Soc.* **2014**, *34*, 925–931. [CrossRef]
25. Liu, Y.; Lin, Y.; Shi, Z.; Nan, C.-W.; Shen, Z. Preparation of $Ca_3Co_4O_9$ and Improvement of Its Thermoelectric Properties by Spark Plasma Sintering. *J. Am. Ceram. Soc.* **2005**, *88*, 1337–1340. [CrossRef]
26. Lee, H.; Vashaee, D.; Wang, D.Z.; Dresselhaus, M.S.; Ren, Z.F.; Chen, G. Effects of Nanoscale Porosity on Thermoelectric Properties of SiGe. *J. Appl. Phys.* **2010**, *107*, 094308. [CrossRef]
27. dos Santos, A.M.; Thomazini, D.; Gelfuso, M.V. Cold Sintering and Thermoelectric Properties of $Ca_3Co_4O_9$ Ceramics. *Ceram. Int.* **2020**, *46*, 14064–14070. [CrossRef]
28. Wang, X.; Suwardi, A.; Zheng, Y.; Zhou, H.; Chien, S.W.; Xu, J. Enhanced Thermoelectric Performance of Nanocrystalline Indium Tin Oxide Pellets by Modulating the Density and Nanoporosity via Spark Plasma Sintering. *ACS Appl. Nano Mater.* **2020**, *3*, 10156–10165. [CrossRef]
29. Hira, U.; Han, L.; Norrman, K.; Christensen, D.V.; Pryds, N.; Sher, F. High-Temperature Thermoelectric Properties of Na- and W-Doped $Ca_3Co_4O_9$ System. *RSC Adv.* **2018**, *8*, 12211–12221. [CrossRef]
30. Kahraman, F.; Madre, M.A.; Rasekh, S.; Salvador, C.; Bosque, P.; Torres, M.A.; Diez, J.C.; Sotelo, A. Enhancement of Mechanical and Thermoelectric Properties of $Ca_3Co_4O_9$ by Ag Addition. *J. Eur. Ceram. Soc.* **2015**, *35*, 3835–3841. [CrossRef]
31. Mele, P.; Kamei, H.; Yasumune, H.; Matsumoto, K.; Miyazaki, K. Development of Thermoelectric Module Based on Dense $Ca_3Co_4O_9$ and $Zn_{0.98}Al_{0.02}O$ Legs. *Met. Mater. Int.* **2014**, *20*, 389–397. [CrossRef]
32. Hira, U.; Ali, S.S.; Latif, S.; Pryds, N.; Sher, F. Improved High-Temperature Thermoelectric Properties of Dual-Doped $Ca_3Co_4O_9$. *ACS Omega* **2022**, *7*, 6579–6590. [CrossRef] [PubMed]
33. Shi, Z.; Xu, J.; Zhu, J.; Zhang, Y.; Gao, T.; Qin, M.; Sun, H.; Dong, G.; Gao, F. Effect of Platelet Template Seeds on Microstructure and Thermoelectric Properties of $Ca_3Co_4O_9$ Ceramics. *Ceram. Int.* **2019**, *45*, 1977–1983. [CrossRef]
34. Mohammed, M.A.; Uday, M.B.; Izman, S. Enhanced Thermoelectric Performance of $Ca_3Co_4O_9$ Doped with Aluminum. *J. Mater. Sci. Mater. Electron.* **2020**, *31*, 16569–16582. [CrossRef]
35. Büttner, G.; Populoh, S.; Xie, W.; Trottmann, M.; Hertrampf, J.; Döbeli, M.; Karvonen, L.; Yoon, S.; Thiel, P.; Niewa, R.; et al. Thermoelectric Properties of $[Ca_2CoO_{3-\delta}][CoO_2]_{1,62}$ as a Function of Co/Ca Defects and Co_3O_4 Inclusions. *J. Appl. Phys.* **2017**, *121*, 215101. [CrossRef]
36. Wu, T.; Tyson, T.A.; Chen, H.; Bai, J.; Wang, H.; Jaye, C. A Structural Change in $Ca_3Co_4O_9$ Associated with Enhanced Thermoelectric Properties. *J. Phys. Condens. Matter* **2012**, *24*, 455602. [CrossRef]
37. Shimoyama, J.I.; Horii, S.; Otzschi, K.; Sano, M.; Kishio, K. Oxygen Nonstoichiometry in Layered Cobaltite $Ca_3Co_4O_y$. *Jpn. J. Appl. Phys.* **2003**, *42*, L194. [CrossRef]

38. Yang, G.; Ramasse, Q.; Klie, R.F. Direct Measurement of Charge Transfer in Thermoelectric $Ca_3Co_4O_9$. *Phys. Rev. B* **2008**, *78*, 153109. [CrossRef]
39. Ahad, A.; Gautam, K.; Majid, S.S.; Francoual, S.; Rahman, F.; De Groot, F.M.F.; Shukla, D.K. Origin of the High Seebeck Coefficient of the Misfit $[Ca_2CoO_3]_{0.62}[CoO_2]$ Cobaltate from Site-Specific Valency and Spin-State Determinations. *Phys. Rev. B* **2020**, *101*, 220202. [CrossRef]
40. Heikes, R.R.; Ure, R.W. Narrow Band Semiconductors, Ionic Crystals, and Liquids. In *Thermoelectricity: Science and Engineering*; Interscience Publishers: New York, NY, USA, 1961; pp. 75–90.
41. Limelette, P.; Hardy, V.; Auban-Senzier, P.; Jérome, D.; Flahaut, D.; Hébert, S.; Frésard, R.; Simon, C.; Noudem, J.; Maignan, A. Strongly Correlated Properties of the Thermoelectric Cobalt Oxide $Ca_3Co_4O_9$. *Phys. Rev. B—Condens. Matter Mater. Phys.* **2005**, *71*, 4–7. [CrossRef]
42. Limelette, P.; Hébert, S.; Muguerra, H.; Frésard, R.; Simon, C. Dual Electronic States in Thermoelectric Cobalt Oxide $[Bi_{1.7}Ca_2O_4]_{0.59}CoO_2$. *Phys. Rev. B* **2008**, *77*, 235118. [CrossRef]
43. Cheng, J.; Sui, Y.; Wang, Y.; Wang, X.; Su, W. First-Order Phase Transition Characteristic of the High Temperature Metal-Semiconductor Transition in $[Ca_2CoO_3]_{0.62}[CoO_2]$. *Appl. Phys. A Mater. Sci. Process.* **2009**, *94*, 911–916. [CrossRef]
44. Wang, Y.; Rogado, N.S.; Cava, R.J.; Ong, N.P. Spin Entropy as the Likely Source of Enhanced Thermopower in $Na_xCo_2O_4$. *Nature* **2003**, *423*, 425–428. [CrossRef] [PubMed]
45. Koshibae, W.; Maekawa, S. Effects of Spin and Orbital Degeneracy on the Thermopower of Strongly Correlated Systems. *Phys. Rev. Lett.* **2001**, *87*, 236603. [CrossRef] [PubMed]
46. Xiang, H.J.; Singh, D.J. Suppression of Thermopower of Na_xCoO_2 by an External Magnetic Field: Boltzmann Transport Combined with Spin-Polarized Density Functional Theory. *Phys. Rev. B* **2007**, *76*, 195111. [CrossRef]
47. Wakisaka, Y.; Hirata, S.; Mizokawa, T.; Suzuki, Y.; Miyazaki, Y.; Kajitani, T. Electronic Structure of $Ca_3Co_4O_9$ Photoemission Spectroscopy: Phase Separation and Charge Localization. *Phys. Rev. B* **2008**, *78*, 235107. [CrossRef]
48. Sugiyama, J.; Brewer, J.H.; Ansaldo, E.J.; Itahara, H.; Dohmae, K.; Seno, Y.; Xia, C.; Tani, T. Hidden Magnetic Transitions in Thermoelectric Layered Cobaltite, $[Ca_2CoO_3]_{0.62}[CoO_2]$. *Phys. Rev. B* **2003**, *68*, 134423. [CrossRef]
49. Terasaki, I.; Tanaka, H.; Satake, A.; Okada, S.; Fujii, T. Out-of-Plane Thermal Conductivity of the Layered Thermoelectric Oxide $Bi_2-xPbxSr_2Co_2O_y$. *Phys. Rev. B* **2004**, *70*, 214106. [CrossRef]